

Article

Spontaneous Formation of a Zincphilic Ag Interphase for Dendrite-Free and Corrosion-Resistant Zinc Metal Anodes

Neng Yu ^{1,2} , Qingpu Zeng ¹, Yiming Fu ¹, Hanbin Li ¹, Jiating Li ¹, Rui Wang ¹, Longlong Meng ¹, Hao Wu ³, Zhuyao Li ¹, Kai Guo ^{1,*} and Lei Wang ^{4,*}

¹ Jiangxi Province Key Laboratory of Functional Organic Polymers, School of Chemistry and Materials Science, East China University of Technology, Nanchang 330013, China; neng063126@ecut.edu.cn (N.Y.); 17870584003@163.com (Q.Z.); 15385663753@163.com (Y.F.); hblj2020@163.com (H.L.); 19970134128@163.com (J.L.); 18352506605@163.com (R.W.); 18293922733@163.com (L.M.); 201860157@ecut.edu.cn (Z.L.)

² Key Laboratory of Advanced Energy Materials Chemistry (Ministry of Education), Nankai University, Tianjin 300071, China

³ State Key Laboratory of Advanced Fiber Materials, Donghua University, Shanghai 201620, China; haowu@hbnu.edu.cn

⁴ State Key Laboratory of Advanced Papermaking and Paper-Based Materials, School of Light Industry Science and Engineering, South China University of Technology, Guangzhou 510641, China

* Correspondence: guokai@ecut.edu.cn (K.G.); felwang@scut.edu.cn (L.W.)

Abstract

The remarkable advantages of zinc anodes render aqueous zinc-ion batteries (ZIBs) a highly promising energy storage solution. Nevertheless, the uncontrolled growth of zinc dendrites and side reactions pose significant obstacles to the practical application of ZIBs. To address these issues, a straightforward strategy has been proposed, involving the addition of a minute quantity of AgNO_3 to the electrolyte to stabilize zinc anodes. This additive spontaneously forms a hierarchically porous Ag interphase on the zinc anodes, which is characterized by its zinc-affinitive nature. The interphase offers abundant zinc nucleation sites and accommodation space, leading to uniform zinc plating/stripping and enhanced kinetics of zinc deposition/dissolution. Moreover, the chemically inert Ag interphase effectively curtails side reactions by isolating water molecules. Consequently, the incorporation of AgNO_3 enables zinc anodes to undergo cycling for extended periods, such as over 4000 h at a current density of 0.5 mA/cm^2 with a capacity of 0.5 mAh/cm^2 , and for 450 h at 2 mA/cm^2 with a capacity of 2 mAh/cm^2 . Full zinc-ion cells equipped with this additive not only demonstrate increased specific capacities but also exhibit significantly improved cycle stability. This research presents a cost-effective and practical approach for the development of reliable zinc anodes for ZIBs.

Keywords: aqueous zinc ion battery; anode; electrolyte additive; zinc dendrite; side reactions



Academic Editor: Hirotoshi Yamada

Received: 20 June 2025

Revised: 17 July 2025

Accepted: 21 July 2025

Published: 24 July 2025

Citation: Yu, N.; Zeng, Q.; Fu, Y.; Li, H.; Li, J.; Wang, R.; Meng, L.; Wu, H.; Li, Z.; Guo, K.; et al. Spontaneous Formation of a Zincphilic Ag Interphase for Dendrite-Free and Corrosion-Resistant Zinc Metal Anodes. *Batteries* **2025**, *11*, 284. <https://doi.org/10.3390/batteries11080284>

Copyright: © 2025 by the authors. Licensee MDPI, Basel, Switzerland. This article is an open access article distributed under the terms and conditions of the Creative Commons Attribution (CC BY) license (<https://creativecommons.org/licenses/by/4.0/>).

1. Introduction

Aqueous zinc ion batteries (ZIBs) are attractive for energy storage due to affordability, safety, non-toxicity, high capacity, and low reaction potential of zinc anodes [1,2]. Yet, their practical use is hindered by the limited cycle life of zinc anodes in aqueous electrolytes, refs. [3–5], caused by uneven zinc nucleation, inhomogeneous ion distribution, and non-uniform electric fields at the zinc/electrolyte interface, leading to dendrite formation [6,7] and hydrogen evolution, which deposits insoluble byproducts and reduces efficiency [8,9]. Efforts to improve zinc anode longevity and prevent dendrites include

structural design [10–12], surface alteration [13–15], separator design [16], and electrolyte engineering [17,18]. Li et al. fabricated a three-dimensional porous Cu foam@Zn anode by electrodepositing zinc on copper foam, effectively reducing local current density and suppressing dendrite growth [12]. However, its complex fabrication process, low volumetric energy density, and large specific surface area-induced side reactions (such as corrosion and hydrogen evolution) hinder its practical application. Liu et al. constructed an in situ zinc hexacyanoferrate (HB-ZnHCF) interphase with large ion channels, strong zinc affinity, and a high Zn^{2+} transference number, which blocks water access, promotes rapid Zn^{2+} transport, and enables uniform zinc deposition [13]. Nevertheless, the mechanically weak and thin interphase is prone to cracking during plating/stripping, eventually leading to dendrite penetration. Cao et al. developed a cellulose nanofiber– ZrO_2 composite separator that regulates uniform deposition via a directional electric field induced by the Maxwell–Wagner polarization effect, effectively inhibiting dendrite growth [19]. However, the use of additional functional separators typically increases ion transport resistance, potentially compromising the rate performance of batteries. Electrolyte engineering, particularly through additive inclusion or special electrolyte formulation, aims to minimize free water. Molecular-crowding, deep eutectic, gel, and solid-state electrolytes aim to solve issues but face challenges like high costs, reduced conductivity, and increased viscosity [20–24].

In contrast, electrolyte additives are low cost and pose no hinder to the electrochemical performance of ZIBs. Electrolyte additives operate through diverse mechanisms. Some additives, such as sodium carboxymethyl cellulose and monosodium glutamate, are used to desolvate Zn^{2+} and thus can suppress water-induced side reactions [25,26]. Organic additives, such as pyridine, L-cysteine, and thiol, preferentially adsorb and form a uniform double electric layer on zinc anodes, which serves as a shielding buffer layer and guides homogeneous zinc ion flux [27,28]. Some reactive additives can deposit on the surface of the zinc anode to form solid electrolyte interfaces, such as ZnF_2/Sn composite, zinc tannin, and zinc–phytic acid complex, which isolates the direct contact of water molecules from the zinc anode and alleviates water involved side reactions [29,30]. However, most additives are unable to simultaneously suppress parasitic reactions and regulate zinc deposition. Design of dual-functional additives is a more favorable solution for the reliable protection of zinc anodes.

In this study, a trace amount of $AgNO_3$ additive is introduced to construct dendrite-free and corrosion-resistant Zn metal anodes. Benefiting from the superior zincophilicity and high electro-conductivity nature of the interphase, the zinc nucleation energy barrier is reduced and kinetics for zinc plating/stripping are improved. More importantly, Ag interphase has a three-dimensional multilevel structure that provides preferential nucleation sites and accommodation space for zinc deposition. Consequently, uniform and dendrite-free zinc deposition with lower zinc deposition overpotentials is observed.

2. Materials and Methods

Electrolytes preparation: Zinc sulfate (ZS) electrolyte with a concentration of 3 mol/L was prepared by dissolving the appropriate weight of $ZnSO_4 \cdot 7H_2O$ in deionized water. Subsequently, an appropriate weight of silver nitrate additive was dissolved in the ZS electrolyte to obtain an $AgNO_3/ZnSO_4$ (AN/ZS) electrolyte containing the desired $AgNO_3$ concentration. The default AN/ZS electrolyte in this paper contains 0.005 mol/L $AgNO_3$ unless specified otherwise. The AN/ZS electrolytes with different concentrations were colorless and transparent solutions (Figure S1).

MnO_2 @graphite paper (MnO_2 @GP) Electrode Preparation: The MnO_2 @GP electrode was deposited by constant current method. First, graphite paper (GP) with a thickness of 50 μm was cut into 4 × 3 cm size. Then, a solution containing 0.1 mol/L $Mn(CHCOO)_2$ and

0.1 mol/L Na₂SO₄ was prepared as the electrodeposition solution. The electrodeposition was carried out in the electrodeposition solution at a current density of 0.5 mA/cm² for 10 min through a three-electrode configuration, in which the GP was used as the working electrode, Pt was the counter electrode, and saturated calomel electrode was the reference electrode. After electrodeposition, the GP was removed and rinsed with deionized water and dried naturally to obtain the MnO₂@GP electrode.

Characterization: The morphology of the zinc anode was characterized by field-emission scanning electron microscopy (SEM). Elemental analysis was obtained using energy dispersive X-ray spectroscopy (EDS). The chemical composition was characterized by X-ray diffractometry (XRD; D8 ADVANCE). X-ray photoelectron spectroscopy (XPS) was performed using a PHI 1600 ESCA (PerkinElmer) instrument. The contact angle of the electrolyte on the surface of zinc anodes was conducted by the Drop Shape Analyzer-DSA25 (KRUESS GmbH, Hamburg, Germany).

Coin cell assembly and electrochemical measurements: Symmetric and full cells were assembled using CR2025 battery cases. For the symmetric cells, pure Zn was used as the electrode, glass fiber as the diaphragm and ZS or AN/ZS as the electrolyte. For the full cell, MnO₂//CC was used as the cathode, pure Zn as the anode, glass fiber as the diaphragm and ZS + 0.1 mol/L MnSO₄ (ZS-M) or AN/ZS + 0.1 mol/L MnSO₄ (AN/ZS-M) aqueous solution as the electrolyte, respectively. Cyclic voltammetry (CV) and constant current charge/discharge (GCD) curves were collected for assembled symmetric and full cells using an electrochemical workstation and NEWARE 4000 test system. The electrochemical impedance spectra (EIS) were tested in the frequency range of 0.01 Hz to 100 kHz with a potential amplitude of 5 mV. Corrosion tests were performed on the Zn anode in a three-electrode system consisting of a pure Zn working electrode, a Zn foil as the counter electrode, and a saturated calomel (SCE) as the reference electrode in the ZS or a AN/ZS electrolyte, respectively. Zinc anodes were tested for corrosion. To observe the growth of zinc dendrites, a transparent symmetric cell was designed for in situ monitoring using an optical microscope and an electrochemical workstation (CHI660E). The transparent cell was constructed by fixing two zinc foils (1 cm × 5 cm) on a glass sheet with a spacing of 1 mm before the two zinc foils, placing a few drops of electrolyte between the two foils, and finally covering the zinc foils with another glass sheet.

Computational Details: All calculations were carried out by using the projector augmented wave method in the framework of the density functional theory (DFT) [31], as implemented in the Vienna *ab-initio* Simulation Package (VASP). The generalized gradient approximation (GGA) and Perdew–Burke–Ernzerhof (PBE) exchange functional was used [32]. The Brillouin zone was sampled by a Monkhorst–Pack to generate k-point mesh of 5 × 5 × 1 for the structure relaxations, while a larger k-grid of 7 × 7 × 1 was generated for the static calculations [33]. The plane-wave energy cutoff was set to 500 eV, and the Monkhorst–Pack method [33] was employed for the Brillouin zone sampling. The convergence criterions of energy and force calculations were set to 10⁻⁵ eV/atom and 0.01 eV Å⁻¹, respectively. To explore the interactions between the Zn atom and substrate (Ag (111), AgZn (111), Ag₂O (111) and Zn (101)) surfaces, the adsorption energies of Zn atom on the substrate surfaces were calculated. A vacuum region of 15 Å is applied to avoid interactions between the neighboring configurations. Here, the adsorption energies (E_a) were calculated by the energy difference of the system after and before adsorption [34]:

$$E_a = E_{\text{Zn-substrate}} - E_{\text{Zn}} - E_{\text{substrate}} \quad (1)$$

where E_{Zn-substrate}, E_{Zn}, and E_{substrate} represent the DFT energies of the Zn adsorbed metal surface, the energy of an isolated Zn atom and the energy of the clean metal surface.

3. Results and Discussion

Figure 1 schematically illustrates the protective mechanism of the Zn anode after introducing AgNO_3 additive into the electrolyte. During cycling, an in situ formed hierarchical porous Ag interfacial phase with high zinc affinity is constructed on the zinc surface. This interfacial phase provides abundant zinc nucleation sites and sufficient accommodation space, promoting uniform Zn deposition/stripping. Moreover, the chemically inert Ag phase effectively suppresses side reactions by isolating water molecules, inhibits dendrite growth and by-product formation, and thus enhances the stability of the zinc anode. AgNO_3 dissolved in 3 mol/L ZnSO_4 electrolyte (ZS) forms the $\text{AgNO}_3/\text{ZnSO}_4$ electrolyte (AN/ZS), depicted in Figure S1. Modified electrolytes containing 1, 3, 5, 8, 10 mmol/L of AgNO_3 are denoted 0.001 M to 0.01 M AN/ZS. The effect of AgNO_3 additive on the zinc deposition behaviors was first studied by examining plated/stripped zinc anodes in the 0.005 M AN/ZS electrolyte. SEM images reveal a flat zinc electrode surface before charging/discharging (Figure 2a). After 20 stripping cycles in ZS electrolyte at $1 \text{ mA}/\text{cm}^2$ for $1 \text{ mAh}/\text{cm}^2$, large platelets form a rough surface by stacking perpendicularly on the electrode (Figure 2b,c) [35]. These platelets, identified as zinc dendrites, are over $20 \mu\text{m}$ thick (Figure 2d), confirmed by pure zinc distribution in energy dispersive spectrometer (EDS) mapping (Figure 2e,f). In contrast, the zinc electrode after 20 stripping cycles in AN/ZS electrolyte lacks perpendicular dendrites, instead showing a uniform layer of particulate matter (Figure 2g). Magnified SEM images indicate these particles have a porous nanosheets structure (Figure 2h). EDS mapping (Figure S2) shows even distribution of Zn and Ag in the particles. XRD analysis post-20th stripping in AN/ZS electrolyte confirms the presence of Ag (JCPDS NO. 04-0783) and a small amount of AgZn (JCPDS NO. 29-1155) and Ag_2O (JCPDS NO. 43-0997) in the coating (Figure 2i). The rapid blackening of the zinc electrode surface upon immersion in AN/ZS is attributed to Ag replacement, with Ag_2O possibly resulting from Ag oxidation by dissolved oxygen [36]. The AgZn alloy minor phase could be the solid solution product of the replacement reaction [37]. The cross-sectional SEM images show that the Ag layer is relatively uniform and about $10 \mu\text{m}$ thick (Figure 2j). EDS characterization reveals an even distribution of Ag and Zn elements in the interphase (Figure 2k,l). According to the literature, Ag has good zincophilicity, and zinc can preferentially nucleate on Ag [38]. The competition effect of Ag suppresses the zinc nucleation on the zinc metal surface [39,40]. And the porous structure of Ag metal particles can provide three-dimensional space to host zinc, therefore alleviating zinc dendrite growth [10–12].

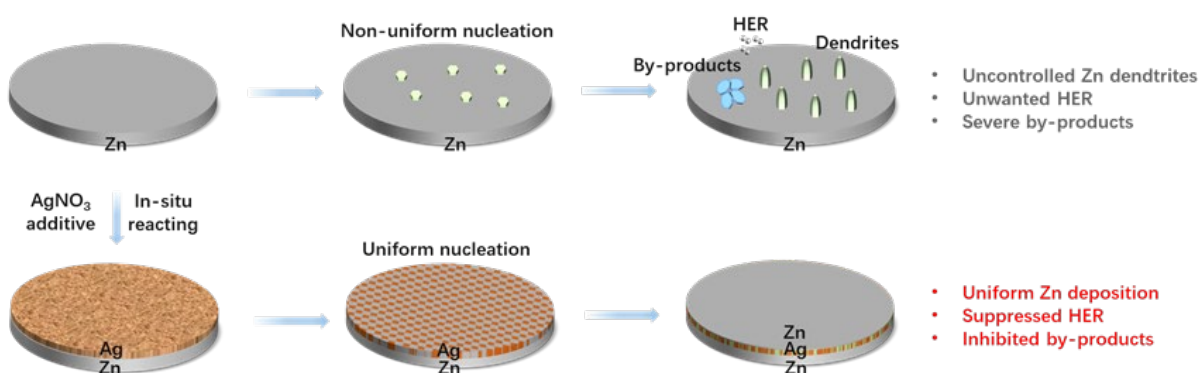


Figure 1. Scheme of Zn anode evolution in the electrolyte without and with the AgNO_3 additive.

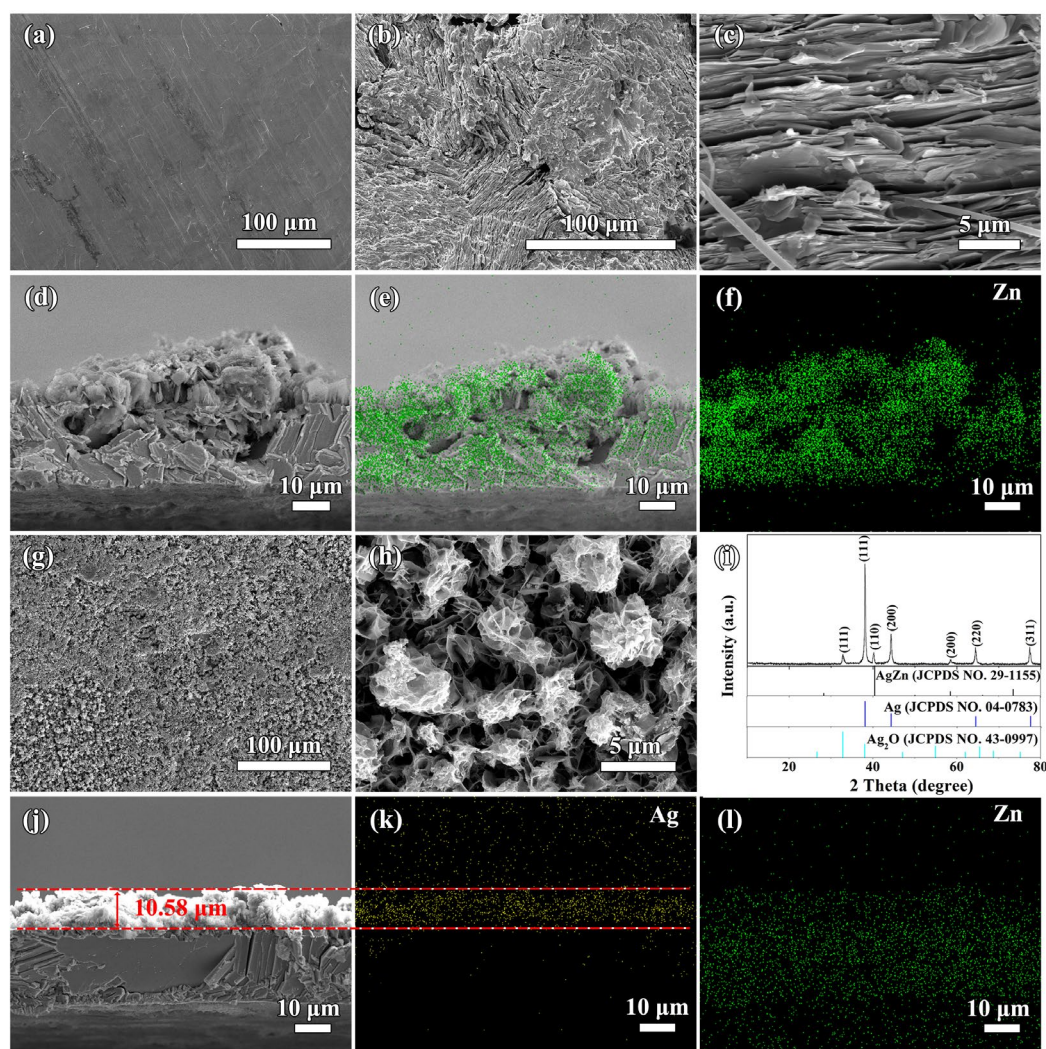


Figure 2. Morphology and composition characterization of Zn anodes in the ZS and 0.005 M AN/ZS electrolytes. **(a)** Surface SEM image of the pristine zinc electrode. **(b,c)** Surface and **(d)** cross-section SEM image, and corresponding EDS mapping of **(e)** all elements and **(f)** Zn element of the zinc electrode after the 20th stripping in the ZS electrolytes at $1 \text{ mA}/\text{cm}^2$ for $1 \text{ mAh}/\text{cm}^2$. **(g,h)** Surface SEM images, **(i)** XRD pattern, **(j)** cross-section SEM image, and corresponding EDS mapping of **(k)** Ag and **(l)** zinc element for the zinc electrode after the 20th stripping in the AN/ZS electrolytes.

The concentration of the additive was optimized. The symmetric cell cycled at $2 \text{ mA}/\text{cm}^2$ with a capacity of $2 \text{ mAh}/\text{cm}^2$ lasted only about 26 h in the pristine ZS electrolyte (Figure 3a), whereas the cell with 0.005 M AN/ZS electrolyte maintained stable cycling for 400 h, which is the longest among all tested additive concentrations and more than 10 times longer than that with the ZS electrolyte. This optimal concentration ensures balanced interfacial behavior during the electrochemical reduction process. At low concentrations below 0.005 M, the amount of Ag^+ is insufficient to form a continuous and compact Ag interfacial phase, resulting in poor nucleation sites and limited suppression of dendrite growth. At high concentrations above 0.005 M, excessive Ag^+ causes an intense displacement reaction with the Zn substrate, leading to uneven Ag deposition, increased interfacial resistance, hindered Zn^{2+} transport, and non-uniform Zn plating. When cycling at $0.5 \text{ mA}/\text{cm}^2$ for $0.5 \text{ mAh}/\text{cm}^2$ in the 0.005 M AN/ZS electrolyte, the polarization voltage is approximately 39 mV, which is significantly lower than that in the ZS electrolyte (~48 mV). This reduction indicates that the AgNO_3 additive effectively lowers the energy barrier for Zn nucleation, promotes more uniform zinc deposition, and suppresses dendrite forma-

tion. Furthermore, a sudden drop in polarization voltage was observed after about 76 h of cycling in the ZS electrolyte, likely due to dendrite-induced short-circuiting caused by uncontrolled Zn dendrite growth. In contrast, the symmetric cell with 0.005 M AN/ZS electrolyte exhibited outstanding cycling stability, operating steadily for over 4500 h (187 days, Figure 3b). These results clearly demonstrate that the AgNO_3 additive effectively inhibits dendrite growth and enhances long-term electrochemical performance. At 5 mA/cm^2 for 1 mAh/cm^2 , the cell cycles for 300 h in the 0.005 M AN/ZS electrolyte, substantially more than the 90 h achieved with the ZS electrolyte (Figure 3c). Additional tests confirm the enhanced stability provided by the 0.005 M AN/ZS electrolyte at other current densities and capacities (Figure S3). Furthermore, the presence of AgNO_3 additive in the electrolyte reduces the overpotential during charge and discharge cycles across various current densities (Figure 3c,d). Tests on Zn//Cu asymmetric cells at 1 mA/cm^2 for 0.5 mAh/cm^2 confirm that lower overpotential and a higher Coulombic efficiency (CE) from 86% to 99.4% for zinc deposition and dissolution are obtained in the 0.005 M AN/ZS electrolyte compared to the ZS electrolyte (Figures S4 and 3e,f). This suggests that zinc dendrite growth and side reactions are minimized and zinc dendrite growth can be attributed to numerous nucleation sites of the hierarchical Ag interphase [41–43]. The maximum cycle life achieved with this method is 4500 h, outperforming recent reports involving other additives or modified zinc anodes (Figure 3g and Table S1) [23,44–52].

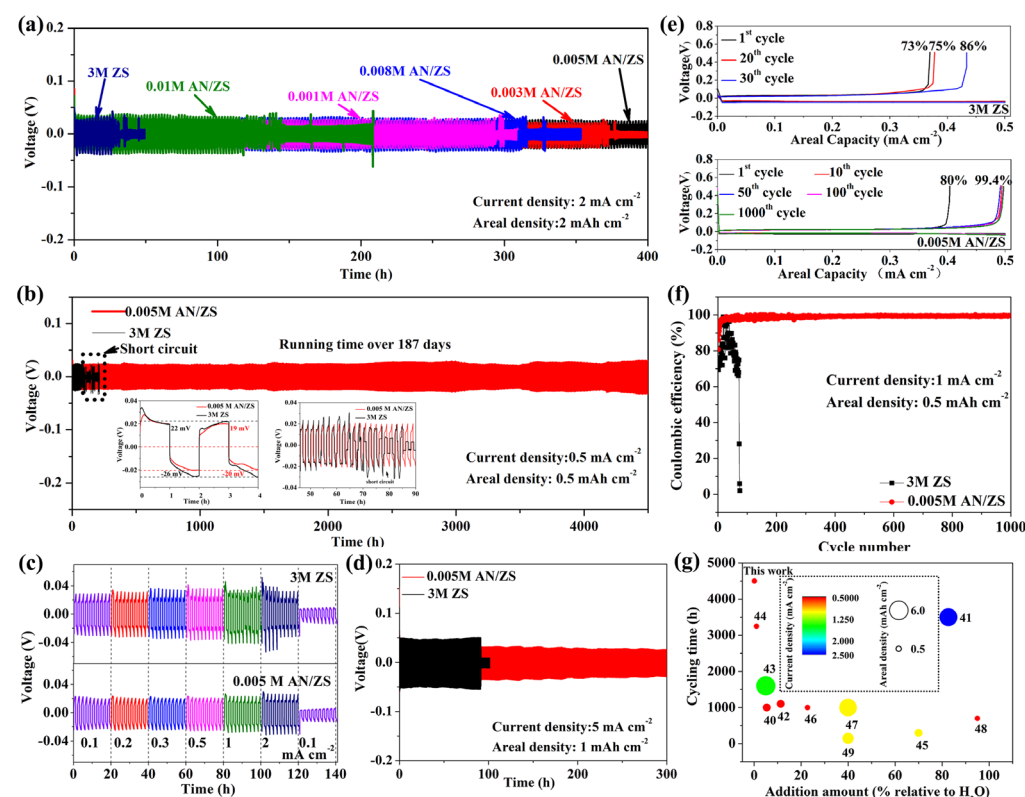


Figure 3. (a) Cycling performance of Zn//Zn symmetrical cell with various electrolytes at 2 mA/cm^2 for 2 mAh/cm^2 and at (b) 1 mA/cm^2 for 0.5 mAh/cm^2 . (c) Rate performance of symmetric cells at $0.1, 0.2, 0.3, 0.5, 1$, and 2 mA/cm^2 . (d) Cycling performance of symmetric cells at 5 mA/cm^2 for 1 mAh/cm^2 . (e) Voltage profiles at various cycles and (f) CE Zn//Cu cell cycling at 1 mA/cm^2 for 0.5 mAh/cm^2 . (g) Performance of Zn symmetric cells with AgNO_3 additive compared with other recently reported additives.

The spontaneously formed Ag interphase acts as a protective layer that can repair damage to the zinc metal surface, as demonstrated through cross-electrolyte and letter-engraving tests. A short-circuited $\text{Zn} \parallel \text{Zn}$ symmetric battery in ZS electrolyte could restore

and resume a long lifespan of 470 h upon reassembly with 0.005 M AN/ZS electrolyte (Figure 4a). Additionally, a zinc electrode, after 80 h of cycling, was etched with the letters “HUT” and then cycled for another 220 h, during which the etching nearly vanished (Figure 4b). These tests suggest that failed ZIBs might be rehabilitated by replacing or supplementing the electrolyte. Investigations into zinc nucleation behavior with AgNO_3 additive showed that zinc anodes exhibit reduced self-corrosion rates and improved corrosion resistance in 0.005 M AN/ZS electrolyte compared to ZS electrolyte (Figure 4c), as evidenced by linear polarization curves (Figure 4d). Hydrogen evolution reaction (HER) overpotential in the 0.005 M AN/ZS electrolyte was found to be significantly higher than in the ZS electrolyte, indicating that the AgNO_3 additive enhances HER overpotential, thereby suppressing HER and the buildup of by-products on zinc anodes [53]. This explains the enhanced reversibility observed in zinc anodes within the 0.005 M AN/ZS electrolyte.

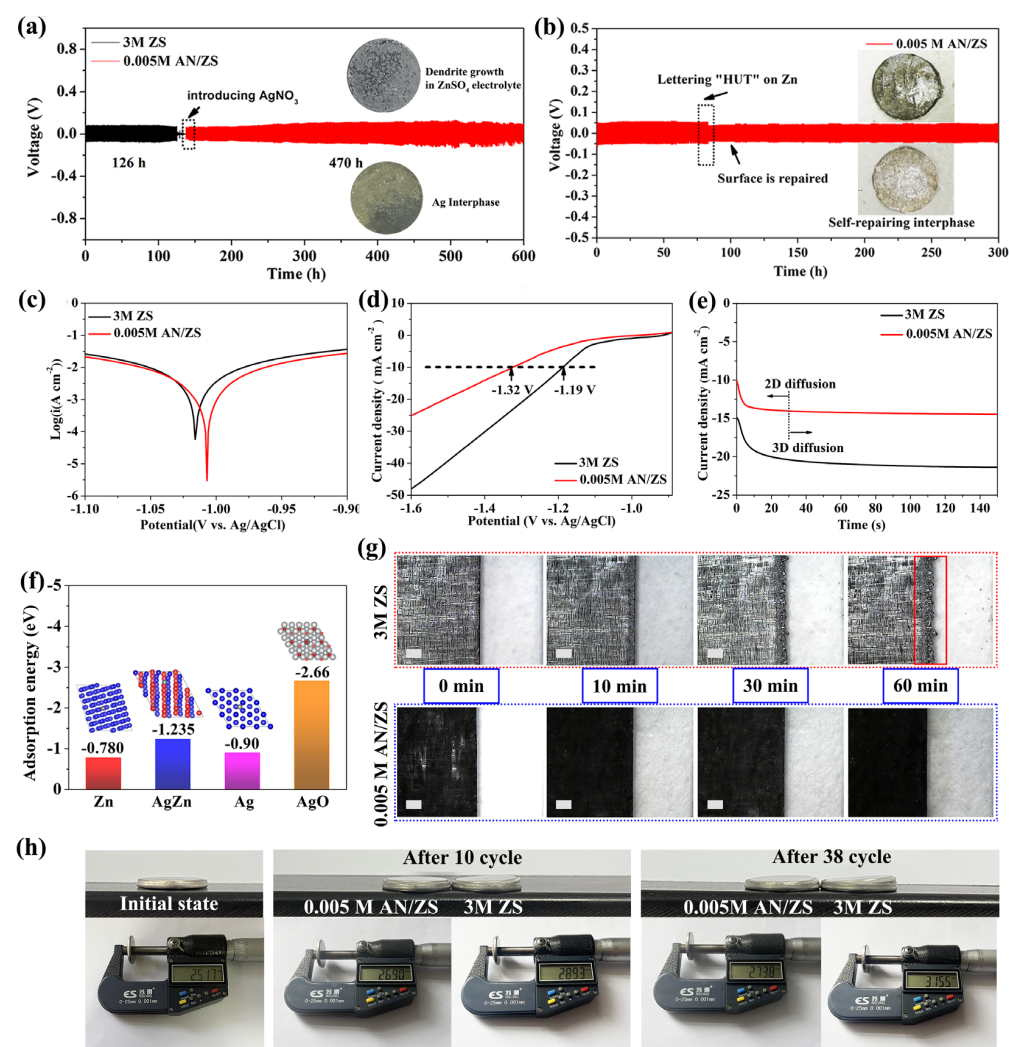


Figure 4. (a) Voltage profiles of $\text{Zn} \parallel \text{Zn}$ symmetrical cells cycling in ZnSO_4 electrolyte for 126 h and then introducing AN under 1 mA cm^{-2} , 0.25 mAh cm^{-2} . (b) Cycling performance of $\text{Zn} \parallel \text{Zn}$ symmetrical cells in 0.005 M AN/ZS electrolyte before and after lettering recombination under 1 mA cm^{-2} , 0.25 mAh cm^{-2} . (c) Linear polarization curves of Zn anodes tested at 10 mV s^{-1} , (d) LSV curves for the Zn anode test at 5 mV s^{-1} , (e) chronoamperometry curves of Zn anode at a -150 mV overpotential in the ZS and 0.005 M AN/ZS electrolyte. (f) The adsorption energies of Zn atom on Zn(101), Ag(111), and Ag_2O (111) surfaces. Inset: corresponding computational models. (g) In situ optical microscope images of the Zn deposition process in ZS and 0.005 M AN/ZS electrolytes at 5 mA cm^{-2} . (h) The photos of symmetrical cells with the ZS and 0.005 M AN/ZS electrolytes after 0 cycles, 10 cycles, and 38 cycles at 0.5 mA cm^{-2} for 0.5 mAh cm^{-2} , respectively.

To assess the impact of the additive on corrosion, zinc electrodes were submerged in both ZS and 0.005 M AN/ZS electrolytes for several days. After one day in ZS electrolyte, the zinc electrode lost its metallic sheen and became rough after six days due to the buildup of white corrosion byproducts (Figure S5). In contrast, zinc in 0.005 M AN/ZS electrolyte turned black rapidly but showed no significant morphological changes over one to six days (Figure S5). SEM images confirm the accumulation of corrosion products on the Zn electrode in ZS electrolyte, whereas the electrode remained unaltered in 0.005 M AN/ZS electrolyte after six days (Figure S6), demonstrating that the additive mitigates zinc anode corrosion. Chronoamperometry (CA) tests at -150 mV were conducted to study the zinc nucleation process. In 0.005 M AN/ZS electrolyte, three-dimensional (3D) zinc ion diffusion occurred shortly after 30 s, converting from two-dimensional (2D) diffusion (Figure 4e). It suggests lateral diffusion of zinc ions upon reaching the electrode surface, which supports homogeneous zinc ion adsorption and plating [54,55]. Conversely, in ZS electrolyte, 2D diffusion persisted for over 140 s, leading to uneven zinc ion adsorption, localized nucleation, and zinc dendrite growth [56].

Theoretical calculations further elucidate zinc ion plating behavior. Zinc adsorption energies on Zn (101), Ag (111), AgZn (111) and Ag_2O (111) surfaces are -0.780 , -0.90 , -1.235 and -2.66 eV, respectively (Figure 4f). Higher adsorption energy on Ag indicates strong zincophilicity, favoring zinc ion deposition on the Ag interphase rather than the Zn surface [54,57]. In addition, the 3D nanostructured interphase accommodates zinc deposition, potentially reducing dendrite formation. Electrochemical impedance tests on Zn/Zn cells reveal that charge transfer impedance (R_{ct}) in 0.005 M AN/ZS electrolyte is approximately 180 Ohms after two hours, rising to around 280 Ohms after 24 h. In ZS electrolyte, R_{ct} values are 440 and 880 Ohms after 2 and 24 h, respectively (Figure S7). This indicates that the Ag-coated electrode resists water-related side reactions and inhibits byproduct growth, likely due to the Ag layer blocking direct water contact. The zinc anode also exhibits improved wettability in 0.005 M AN/ZS electrolyte, as seen by a smaller contact angle (Figure S8), facilitating faster zinc deposition kinetics [58].

Transparent cells allowed direct observation of zinc deposition in various electrolytes. After 30 min in ZS electrolyte, protrusions formed on the zinc anode, growing larger by 60 min. However, in 0.005 M AN/ZS electrolyte, the zinc anode stayed unchanged with no dendrite growth, even after 60 min (Figure 4g). This highlights the effectiveness of the Ag interface at inhibiting zinc dendrites. The hydrogen evolution reaction (HER) was assessed by measuring changes in cell thickness (Figure 4h). After 38 cycles, the symmetric cell with 0.005 M AN/ZS electrolyte showed an 8.8% increase in thickness, remaining sealed. Conversely, the cell with ZS electrolyte expanded by 25.3%, causing buckling and opening the coin cell. This suggests that 0.005 M AN/ZS electrolyte effectively curbs HER due to the addition of AgNO_3 [59,60]. Post-HER optical images (Figure S9) revealed uneven zinc deposition after 38 cycles in ZS electrolyte but a stable anode surface in 0.005 M AN/ZS electrolyte. This indicates that 0.005 M AN/ZS significantly reduces by-products, which is beneficial for high coulombic efficiency and uniform zinc plating.

The 0.005 M AN/ZS electrolyte proved feasible in full cell electrochemical tests. The $\text{MnO}_2@\text{GP}$ cathode was made by depositing MnO_2 on graphite paper (Figure S10). Full cells included this cathode, a zinc anode, a glass fiber separator, and aqueous electrolyte. The full cell has a similar CV curve in 0.005 M AN/ZS electrolytes but with higher current densities (Figure 5a). Tests show the full cell has larger discharge capacities at 0.5 to 5 A/g in the 0.005 M AN/ZS electrolyte (Figure 5b,c). After 2000 cycles at 2 A/g, the cell with 0.005 M AN/ZS electrolyte retained 83% of their capacity with a stable 100% coulombic efficiency, while the cell ZS electrolyte retains only 55% of initial capacity (Figure 5d). The 0.005 M AN/ZS electrolyte cells demonstrated better cycling stability and reversibility,

outperforming other additives in recent studies (Table S2). The lowered the charge transfer resistance in the modified electrolyte can improve zinc deposition and dissolution kinetics (Figure 5e). Compared to the ZS electrolyte, 0.005 M AN/ZS electrolyte significantly reduces the charge transfer resistance (R_{ct}) from 124.6 Ω to 54.2 Ω , demonstrating its effectiveness in lowering interfacial resistance and enhancing charge transport capability. To further investigate the kinetic behavior of the Zn//MnO₂ cell, we have calculated the Zn²⁺ diffusion coefficient (D_R) from the EIS curves. The calculated diffusion coefficients are summarized in Table S3. Notably, the 0.005 M AN/ZS electrolyte exhibits a higher D_R than the ZS electrolyte, indicating that the introduction of AgNO₃ effectively enhances charge transfer kinetics and facilitates Zn²⁺ diffusion.

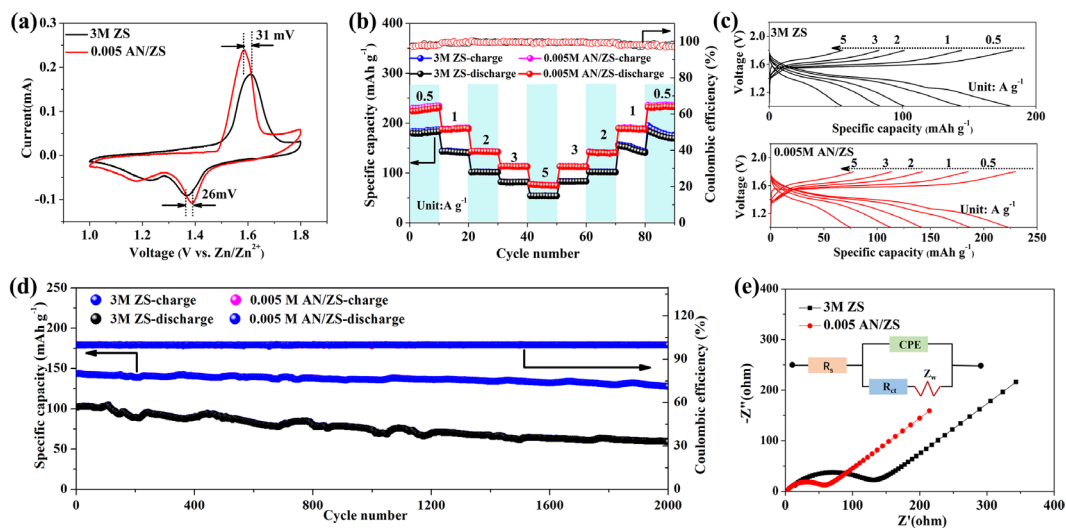


Figure 5. Electrochemical behavior of Zn//MnO₂ full cell with the ZS and 0.005 M AN/ZS electrolytes. (a) CV curves at 0.1 mV/s, (b) rate performance, and (c) charge–discharge curves at different current densities. (d) Long-term cycling stability and efficiency at 2 A/g. (e) Electrochemical impedance spectroscopy after 2000 cycles.

4. Conclusions

In summary, a stable zinc anode was realized by adding a trace amount of AgNO₃ additive to the electrolyte. The optimal concentration of AgNO₃ additive has been disclosed to be 5 mmol/L. The AgNO₃ additive reacted in situ on the zinc anode to construct a self-repairing hierarchically porous and zincophilic Ag interphase, which serves as a zinc nucleation site and provides abundant space to accommodate plated zinc, thus enhancing the deposition/dissolution kinetics of zinc and inhibiting the growth of zinc dendrites. The inert Ag interphase effectively inhibits the HER and formation of by-products, thus ensuring excellent stability and reversibility. Due to the protection of the interphase, the cycle life of the symmetric cell with the additive is as high as 450 h, which is much higher than 30 h without the additive at 2 mA/cm² for 2 mAh/cm². At 1 mA/cm² for 0.5 mAh/cm², the introduction of additives allows symmetric cells to be cycled for more than 4000 h. In addition, full cells based on MnO₂@GP cathode exhibit not only higher capacities and better rate performance but also show significantly improved cycle stability in the 0.005 M AN/ZS electrolyte. This work provides a large-scale, cost-effective, and feasible path for obtaining long life-span and dendrite-free anodes for ZIBs.

Supplementary Materials: The following supporting information can be downloaded at: <https://www.mdpi.com/article/10.3390/batteries11080284/s1>, Figure S1: Photos of the AN/ZS electrolytes with AgNO₃ additive at various concentration ranges from 0 to 0.01 mol/L; Figure S2: EDX mapping of zinc electrode after 20 cycles in the AN/ZS electrolyte. (a,b) SEM image, (c) Zn element mapping,

and (d) Ag element mapping; Figure S3: Plating/stripping cycling stability of Zn symmetric cells in the ZS and the AN/ZS electrolytes under (a) 1 mA cm^{-2} and 0.5 mAh cm^{-2} , (b) 5 mA cm^{-2} and 5 mAh cm^{-2} ; Figure S4: Nucleation overpotentials of Zn deposition on Cu matrixes in the ZS and the AN/ZS electrolytes at different current densities of (a) 0.5 mA cm^{-2} , (b) 1 mA cm^{-2} and (c) 2 mA cm^{-2} , (d) histogram comparisons of corresponding nucleation overpotentials; Figure S5: The stability of Zn foil in different electrolytes. (a) Zn foil soaked in the ZS electrolyte. (b–e) Zn metal before soaking in the ZS electrolyte and after soaking in electrolyte for 1, 2, and 6 days, respectively. (f–i) Zn metal before soaking in the AN/ZS electrolyte and after soaking in electrolyte for 1, 2, and 6 days, respectively; Figure S6: SEM images of Zn foil. Zn foil soaked in the ZS electrolyte for (a) 1 day. (b) 6 days. Zn foil soaked in the AN/ZS electrolytes for (c) 1 day and (d) 6 days; Figure S7: Nyquist plots of the Zn//Zn symmetric cells in the ZS and the AN/ZS electrolytes after resting at different times; Figure S8: Contact angle measurements of Zn anode in the ZS and AN/ZS electrolytes; Figure S9: Digital images of Zinc anode after 10 cycles and 38 cycles, (a,b) in the ZS, (c,d) AN/ZS electrolytes; Figure S10: Characterization of the $\text{MnO}_2@\text{GP}$ electrode: (a,b) SEM image. XPS spectra for MnO_2 , (c) XPS survey of MnO_2 , and resolution spectra of (d) Mn 3s, (e) Mn2p, and (f) O1s; Table S1: Comparison of electrochemical performances with recently modified Zn-Zn symmetric cell strategies; Table S2: Comparison of electrochemical performances of aqueous zinc-ion batteries assembled with MnO_2 cathodes based on different additives for suppressing Zn dendrite with previously reported works; Table S3: R_s , R_{ct} , σ and D_R Values determined from the EIS spectra.

Author Contributions: Conceptualization, N.Y. and K.G.; software, J.L.; investigation, N.Y., Q.Z., H.L., R.W. and L.M.; resources, Z.L. and H.W.; data curation, N.Y., Q.Z. and Y.F.; writing—original draft preparation, N.Y.; writing—review and editing, K.G. and L.W.; visualization, J.L.; supervision, K.G. and L.W. All authors have read and agreed to the published version of the manuscript.

Funding: This research was funded by the National Natural Science Foundation of China (52102214, Kai Guo), the Jiangxi Provincial Natural Science Foundation (20242BAB25162, Kai Guo 20224BAB203016, Neng Yu), the China Scholarship Council program (Project No.: 202300880001, Neng Yu), the National (Jiangxi Province) College Students Innovation and Entrepreneurship Training Program (S202510405050, Yiming Fu). The State Key Laboratory of Advanced Fiber Materials (KF2501, Hao Wu).

Data Availability Statement: The original contributions presented in the study are included in the article/Supplementary Materials, further inquiries can be directed to the corresponding author.

Acknowledgments: The authors thank SCI-GO (www.sci-go.com, accessed on 12 January 2025) and Shyanjia Lab (www.shyanjia.com, accessed on 15 March 2025) for the material characterization service.

Conflicts of Interest: The authors declare no conflicts of interest.

References

1. Senguttuvan, P.; Han, S.-D.; Kim, S.; LipsonA, L.; Tepavcevic, S.; Fister, T.T.; Bloom, I.D.; Burrell, A.K.; Johnson, C.S. A High Power Rechargeable Nonaqueous Multivalent Zn/ V_2O_5 Battery. *Adv. Energy Mater.* **2016**, *6*, 1600826. [[CrossRef](#)]
2. Zhang, L.; Xiao, J.; Xiao, X.; Xin, W.; Geng, Y.; Yan, Z.; Zhu, Z. Molecular engineering of self-assembled monolayers for highly utilized Zn anodes. *eScience* **2024**, *4*, 100205. [[CrossRef](#)]
3. Yuan, L.; Hao, J.; Johannessen, B.; Ye, C.; Yang, F.; Wu, C.; Dou, S.; Liu, H.; Qiao, S. Hybrid working mechanism enables highly reversible Zn electrodes. *eScience* **2023**, *3*, 100096. [[CrossRef](#)]
4. Al-Abbasi, M.; Zhao, Y.; He, H.; Liu, H.; Xia, H.; Zhu, T.; Wang, K.; Xu, Z.; Wang, H.; Zhang, W.; et al. Challenges and protective strategies on zinc anode toward practical aqueous zinc-ion batteries. *Carbon Neutral.* **2024**, *3*, 108–141. [[CrossRef](#)]
5. Xue, T.; Mu, Y.; Wei, X.; Zhou, Z.; Zhou, Y.; Zhang, Z.; Yang, C.; Qiu, J.; Zang, L.; Zeng, L. From Fundamentals to Practice: Electrolyte Strategies for Zinc-Ion Batteries in Extreme Temperature. *Carbon Neutral.* **2025**, *4*, e183. [[CrossRef](#)]
6. Li, Q.; Chen, A.; Wang, D.; Zhao, Y.; Wang, X.; Jin, X.; Xiong, B.; Zhi, C. Tailoring the metal electrode morphology via electrochemical protocol optimization for long-lasting aqueous zinc batteries. *Nat. Commun.* **2022**, *13*, 3699. [[CrossRef](#)] [[PubMed](#)]
7. Chen, F.; Huang, K.; Li, H.; Zhong, Q.; Yue, J.; Diao, J.; Wang, Z.; Huang, G.; Jiang, B.; Pan, F. Interlayer Cationic Defect Engineering in Lamellar Vanadate Cathodes Enables Ultralong-Lifespan Magnesium-Ion Batteries. *ACS Energy Lett.* **2025**, *10*, 2052–2060. [[CrossRef](#)]

8. Yu, H.; Chen, Y.; Wei, W.; Ji, X.; Chen, L. A Functional Organic Zinc-Chelate Formation with Nanoscaled Granular Structure Enabling Long-Term and Dendrite-Free Zn Anodes. *ACS Nano* **2022**, *16*, 9736–9747. [[CrossRef](#)]
9. Wei, S.; Qi, Z.-H.; Xia, Y.; Chen, S.; Wang, C.; Wang, Y.; Zhang, P.; Zhu, K.; Cao, Y.; Guo, X.; et al. Monolayer Thiol Engineered Covalent Interface toward Stable Zinc Metal Anode. *ACS Nano* **2022**, *16*, 21152–21162. [[CrossRef](#)]
10. Jian, Q.; Guo, Z.; Zhang, L.; Wu, M.; Zhao, T. A hierarchical porous tin host for dendrite-free, highly reversible zinc anodes. *Chem. Eng. J.* **2021**, *425*, 130643. [[CrossRef](#)]
11. Fan, X.; Yang, H.; Wang, X.; Han, J.; Wu, Y.; Gou, L.; Li, D.-L.; Ding, Y.-L. Enabling Stable Zn Anode via a Facile Alloying Strategy and 3D Foam Structure. *Adv. Mater. Interfaces* **2021**, *8*, 2002184. [[CrossRef](#)]
12. Li, C.; Shi, X.; Liang, S.; Ma, X.; Han, M.; Wu, X.; Zhou, J. Spatially homogeneous copper foam as surface dendrite-free host for zinc metal anode. *Chem. Eng. J.* **2020**, *379*, 122248. [[CrossRef](#)]
13. Liu, M.; Yuan, W.; Ma, G.; Qiu, K.; Nie, X.; Liu, Y.; Shen, S.; Zhang, N. In-Situ Integration of a Hydrophobic and Fast-Zn²⁺-Conductive Inorganic Interphase to Stabilize Zn Metal Anodes. *Angew. Chem. Int. Ed.* **2023**, *62*, e202304444. [[CrossRef](#)] [[PubMed](#)]
14. Zhang, S.; Ye, M.; Zhang, Y.; Tang, Y.; Liu, X.; Li, C.C. Regulation of Ionic Distribution and Desolvation Activation Energy Enabled by In Situ Zinc Phosphate Protective Layer toward Highly Reversible Zinc Metal Anodes. *Adv. Funct. Mater.* **2023**, *33*, 2208230. [[CrossRef](#)]
15. Yu, N.; Li, Y.; She, W.; Li, H.; Chen, H.; Cheng, W.; Chen, J.; Liu, H.; Tu, Y.; Huang, Z.; et al. Binder-Free Sodium Zinc Phosphate Protection Layer Enabled Dendrite-Free Zn Metal Anode. *ACS Appl. Mater. Interfaces* **2022**, *14*, 50827–50835. [[CrossRef](#)] [[PubMed](#)]
16. Li, C.; Sun, Z.; Yang, T.; Yu, L.; Wei, N. Directly grown vertical graphene carpets as janus separators toward stabilized Zn metal anodes. *Adv. Mater.* **2020**, *32*, 2003425. [[CrossRef](#)]
17. Li, C.; Kingsbury, R.; Thind, A.S.; Shyamsunder, A.; Fister, T.T.; Klie, R.F.; Persson, K.A.; Nazar, L.F. Enabling selective zinc-ion intercalation by a eutectic electrolyte for practical anodeless zinc batteries. *Nat. Commun.* **2023**, *14*, 3067. [[CrossRef](#)]
18. Zhong, Y.; Xie, X.; Zeng, Z.; Lu, B.; Chen, G.; Zhou, J. Triple-function Hydrated Eutectic Electrolyte for Enhanced Aqueous Zinc Batteries. *Angew. Chem. Int. Ed.* **2023**, *62*, e202310577. [[CrossRef](#)]
19. Cao, J.; Zhang, D.; Gu, C.; Zhang, X.; Okhawilai, M.; Wang, S.; Han, J.; Qin, J.; Huang, Y. Modulating Zn deposition via ceramic-cellulose separator with interfacial polarization effect for durable zinc anode. *Nano Energy* **2021**, *89*, 106322. [[CrossRef](#)]
20. Chen, S.; Lan, R.; Humphreys, J.; Tao, S. Salt-concentrated acetate electrolytes for a high voltage aqueous Zn/MnO₂ battery. *Energy Storage Mater.* **2020**, *28*, 205–215. [[CrossRef](#)]
21. Wang, L.; Yu, H.; Chen, D.; Jin, Y.; Jiang, L.; He, H.; Zhou, G.; Xie, Z.; Chen, Y. Steric hindrance and orientation polarization by a zwitterionic additive to stabilize zinc metal anodes. *Carbon Neutral.* **2024**, *3*, 996–1008. [[CrossRef](#)]
22. Han, D.; Sun, T.; Zhang, R.; Zhang, W.; Ma, T.; Du, H.; Wang, Q.; He, D.; Zheng, S.; Tao, Z. Eutectic Electrolytes with Doubly-Bound Water for High-Stability Zinc Anodes. *Adv. Funct. Mater.* **2022**, *32*, 2209065. [[CrossRef](#)]
23. Tang, Y.; Li, J.-H.; Xu, C.-L.; Liu, M.; Xiao, B.; Wang, P.-F. Electrode/electrolyte interfacial engineering for aqueous Zn-ion batteries. *Carbon Neutral.* **2023**, *2*, 186–212. [[CrossRef](#)]
24. Zhi, J.; Zhao, S.; Zhou, M.; Wang, R.; Huang, F. A zinc-conducting chalcogenide electrolyte. *Sci. Adv.* **2023**, *9*, eade2217. [[CrossRef](#)] [[PubMed](#)]
25. Huang, H.; Yun, J.; Feng, H.; Tian, T.; Xu, J.; Li, D.; Xia, X.; Yang, Z.; Zhang, W. Towards high-performance zinc anode for zinc ion hybrid capacitor: Concurrently tailoring hydrodynamic stability, zinc deposition and solvation structure via electrolyte additive. *Energy Storage Mater.* **2023**, *55*, 857–866. [[CrossRef](#)]
26. Zhong, Y.; Cheng, Z.; Zhang, H.; Li, J.; Liu, D.; Liao, Y.; Meng, J.; Shen, Y.; Huang, Y. Monosodium glutamate, an effective electrolyte additive to enhance cycling performance of Zn anode in aqueous battery. *Nano Energy* **2022**, *98*, 107220. [[CrossRef](#)]
27. Luo, J.; Xu, L.; Zhou, Y.; Yan, T.; Shao, Y.; Yang, D.; Zhang, L.; Xia, Z.; Wang, T.; Zhang, L.; et al. Regulating the Inner Helmholtz Plane with a High Donor Additive for Efficient Anode Reversibility in Aqueous Zn-Ion Batteries. *Angew. Chem. Int. Ed.* **2023**, *135*, e202302302. [[CrossRef](#)]
28. Li, D.; Tang, Y.; Liang, S.; Lu, B.; Chen, G.; Zhou, J. Self-assembled multilayers direct a buffer interphase for long-life aqueous zinc-ion batteries. *Energy Environ. Sci.* **2023**, *16*, 3381–3390. [[CrossRef](#)]
29. Zhou, Y.; Tong, H.; Wu, Y.; Chen, X.; Wu, C.; Xu, Z.; Shen, L.; Zhang, X. A Dendrite-Free Zn Anode Co-modified with In and ZnF₂ for Long-Life Zn-Ion Capacitors. *ACS Appl. Mater. Interfaces* **2022**, *14*, 46665–46672. [[CrossRef](#)]
30. Zhang, P.-F.; Wu, Z.; Zhang, S.-J.; Liu, L.-Y.; Tian, Y.; Dou, Y.; Lin, Z.; Zhang, S. Tannin acid induced anticorrosive film toward stable Zn-ion batteries. *Nano Energy* **2022**, *102*, 107721. [[CrossRef](#)]
31. Liu, H.; Wang, J.-G.; Hua, W.; Ren, L.; Sun, H.; Hou, Z.; Huyan, Y.; Cao, Y.; Wei, C.; Kang, F. Navigating fast and uniform zinc deposition via a versatile metal–organic complex interphase. *Energy Environ. Sci.* **2022**, *15*, 1872–1881. [[CrossRef](#)]
32. Kohn, W.; Sham, L.J. Self-Consistent Equations Including Exchange and Correlation Effects. *Phys. Rev.* **1965**, *140*, A1133–A1138. [[CrossRef](#)]
33. Monkhorst, H.J.; Pack, J.D. Special points for Brillouin-zone integrations. *Phys. Rev. B* **1976**, *16*, 1746. [[CrossRef](#)]

34. Lv, X.; Xu, Z.; Li, J.; Chen, J.; Liu, Q. Investigation of fluorine adsorption on nitrogen doped MgAl₂O₄ surface by first-principles. *Appl. Surf. Sci.* **2016**, *376*, 97–104. [CrossRef]
35. Zhang, W.; Dai, Y.; Chen, R.; Xu, Z.; Li, J.; Zong, W.; Li, H.; Li, Z.; Zhang, Z.; Zhu, J.; et al. Highly Reversible Zinc Metal Anode in a Dilute Aqueous Electrolyte Enabled by a pH Buffer Additive. *Angew. Chem. Int. Ed.* **2023**, *135*, e202212695. [CrossRef]
36. Lu, Q.; Liu, C.; Du, Y.; Wang, X.; Ding, L.; Omar, A.; Mikhailova, D. Uniform Zn Deposition Achieved by Ag Coating for Improved Aqueous Zinc-Ion Batteries. *ACS Appl. Mater. Interfaces* **2021**, *13*, 16869–16875. [CrossRef] [PubMed]
37. Wang, Y.; Chen, Y.; Liu, W.; Ni, X.; Qing, P.; Zhao, Q.; Wei, W.; Ji, X.; Ma, J.; Chen, L. Uniform and dendrite-free zinc deposition enabled by in situ formed AgZn₃ for the zinc metal anode. *J. Mater. Chem. A* **2021**, *9*, 8452–8461. [CrossRef]
38. Zhang, Y.; Howe, J.D.; Ben-Yoseph, S.; Wu, Y.; Liu, N. Unveiling the Origin of Alloy-Seeded and Nondendritic Growth of Zn for Rechargeable Aqueous Zn Batteries. *ACS Energy Lett.* **2021**, *6*, 404–412. [CrossRef]
39. Park, J.B.; Choi, C.; Jung, S.W.; Min, B.C.; Park, J.H.; Kim, D.-W. Designing Chemically Replaced Interfacial Layer via Unveiling The Influence of Zn Crystal Facets for Practical Zn-Metal Anodes. *Adv. Mater.* **2024**, *36*, 2308684. [CrossRef]
40. Kim, H.J.; Kim, S.; Heo, K.; Lim, J.; Yashiro, H.; Shin, H.; Jung, H.; Lee, Y.M.; Myung, S. Gold-Nanolayer-Derived Zincophilicity Suppressing Metallic Zinc Dendrites and Its Efficacy in Improving Electrochemical Stability of Aqueous Zinc-Ion Batteries. *Adv. Mater.* **2024**, *36*, 2308592. [CrossRef]
41. Zhou, L.; Yang, F.; Zeng, S.; Gao, X.; Liu, X.; Cao, X.; Yu, P.; Lu, X. Zincophilic Cu Sites Induce Dendrite-Free Zn Anodes for Robust Alkaline/Neutral Aqueous Batteries. *Adv. Funct. Mater.* **2022**, *32*, 2110829. [CrossRef]
42. Ma, C.; Wang, X.; Lu, W.; Wang, C.; Yue, H.; Sun, G.; Zhang, D.; Du, F. Achieving stable Zn metal anode via a simple NiCo layered double hydroxides artificial coating for high performance aqueous Zn-ion batteries. *Chem. Eng. J.* **2022**, *429*, 132576. [CrossRef]
43. Mu, Y.; Zhou, T.; Li, D.; Liu, W.; Jiang, P.; Chen, L.; Zhou, H.; Ge, G. Highly stable and durable Zn-metal anode coated by bi-functional protective layer suppressing uncontrollable dendrites growth and corrosion. *Chem. Eng. J.* **2022**, *430*, 132839. [CrossRef]
44. Liu, M.; Yao, L.; Ji, Y.; Zhang, M.; Gan, Y.; Cai, Y.; Li, H.; Zhao, W.; Zhao, Y.; Zou, Z.; et al. Nanoscale Ultrafine Zinc Metal Anodes for High Stability Aqueous Zinc Ion Batteries. *Nano Lett.* **2023**, *23*, 541–549. [CrossRef]
45. Sun, Y.; Xu, Z.; Xu, X.; Nie, Y.; Tu, J.; Zhou, A.; Zhang, J.; Qiu, L.; Chen, F.; Xie, J.; et al. Low-cost and long-life Zn/Prussian blue battery using a water-in-ethanol electrolyte with a normal salt concentration. *Energy Storage Mater.* **2023**, *48*, 192–204. [CrossRef]
46. Ma, G.; Miao, L.; Dong, Y.; Yuan, W.; Nie, X.; Di, S.; Wang, Y.; Wang, L.; Zhang, N. Reshaping the electrolyte structure and interface chemistry for stable aqueous zinc batteries. *Energy Storage Mater.* **2022**, *47*, 203–210. [CrossRef]
47. Chang, N.; Li, T.; Li, R.; Wang, S.; Yin, Y.; Zhang, H.; Li, X. An aqueous hybrid electrolyte for low-temperature zinc-based energy storage devices. *Energy Environ. Sci.* **2020**, *13*, 3527–3535. [CrossRef]
48. Cao, L.; Li, D.; Hu, E.; Xu, J.; Deng, T.; Ma, L.; Wang, Y.; Yang, X.-Q.; Wang, C. Solvation Structure Design for Aqueous Zn Metal Batteries. *J. Am. Chem. Soc.* **2020**, *142*, 21404–21409. [CrossRef]
49. Miao, L.; Wang, R.; Di, S.; Qian, Z.; Zhang, L.; Xin, W.; Liu, M.; Zhu, Z.; Chu, S.; Du, Y.; et al. Aqueous Electrolytes with Hydrophobic Organic Cosolvents for Stabilizing Zinc Metal Anodes. *ACS Nano* **2022**, *16*, 9667–9678. [CrossRef]
50. Liu, Z.; Wang, R.; Ma, Q.; Wan, J.; Zhang, S.; Zhang, L.; Li, H.; Luo, Q.; Wu, J.; Zhou, T.; et al. A Dual-Functional Organic Electrolyte Additive with Regulating Suitable Overpotential for Building Highly Reversible Aqueous Zinc Ion Batteries. *Adv. Funct. Mater.* **2023**, *34*, 2214538. [CrossRef]
51. Li, T.C.; Lim, Y.; Li, X.L.; Luo, S.; Lin, C.; Fang, D.; Xia, S.; Wang, Y.; Yang, H.Y. A Universal Additive Strategy to Reshape Electrolyte Solvation Structure toward Reversible Zn Storage. *Adv. Energy Mater.* **2022**, *12*, 2103231. [CrossRef]
52. Li, C.; Kingsbury, R.; Zhou, L.; Shyamsunder, A.; Persson, K.A.; Nazar, L.F. Tuning the Solvation Structure in Aqueous Zinc Batteries to Maximize Zn-Ion Intercalation and Optimize Dendrite-Free Zinc Plating. *ACS Energy Lett.* **2022**, *7*, 533–540. [CrossRef]
53. Wang, M.; Meng, Y.; Li, K.; Ahmad, T.; Chen, N.; Xu, Y.; Sun, J.; Chuai, M.; Zheng, X.; Yuan, Y.; et al. Toward dendrite-free and anti-corrosion Zn anodes by regulating a bismuth-based energizer. *eScience* **2022**, *2*, 509–517. [CrossRef]
54. Liu, C.; Luo, Z.; Deng, W.; Wei, W.; Chen, L.; Pan, A.; Ma, J.; Wang, C.; Zhu, L.; Xie, L.; et al. Liquid Alloy Interlayer for Aqueous Zinc-Ion Battery. *ACS Energy Lett.* **2021**, *6*, 675–683. [CrossRef]
55. Zheng, J.; Huang, Z.; Zeng, Y.; Liu, W.; Wei, B.; Qi, Z.; Wang, Z.; Xia, C.; Liang, H. Electrostatic Shielding Regulation of Magnetron Sputtered Al-Based Alloy Protective Coatings Enables Highly Reversible Zinc Anodes. *Nano Lett.* **2022**, *22*, 1017–1023. [CrossRef] [PubMed]
56. Ren, J.; Li, C.; Zhang, S.; Luo, B.; Tian, M.; Liu, S.; Wang, L. Mass-producible in-situ amorphous solid/electrolyte interface with high ionic conductivity for long-cycling aqueous Zn-ion batteries. *J. Colloid Interface Sci.* **2023**, *641*, 229–238. [CrossRef]
57. Han, C.; Li, W.; Liu, H.K.; Dou, S.; Wang, J. Principles and strategies for constructing a highly reversible zinc metal anode in aqueous batteries. *Nano Energy* **2020**, *74*, 104880. [CrossRef]
58. Li, X.; Wang, M.; Wang, H.; Gao, Y.; Tang, Z.; Wang, J.; Feng, Y.; Yang, Z.; Zhou, D.; Chen, J.; et al. Regulation and Stabilization of the Zinc Metal Anode Interface by Electroless Plating of a Multifunctionalized Polydopamine Layer. *ACS Appl. Mater. Interfaces* **2022**, *14*, 43215–43225. [CrossRef]

59. Lu, H.; Hu, J.; Wei, X.; Zhang, K.; Xiao, X.; Zhao, J.; Hu, Q.; Yu, J.; Zhou, G.; Xu, B. A recyclable biomass electrolyte towards green zinc-ion batteries. *Nat. Commun.* **2023**, *14*, 4435. [[CrossRef](#)]
60. Zhou, J.; Peng, M.; Xia, X.; Qian, S.; Wang, Z.; Zhu, C.; Zeng, X.; Ji, H.; Wang, S.; Zhou, X.; et al. New Type of Dynamically ‘Solid–Liquid’ Interconvertible Electrolyte for High-Rate Zn Metal Battery. *Nano Lett.* **2022**, *22*, 2898–2906. [[CrossRef](#)]

Disclaimer/Publisher’s Note: The statements, opinions and data contained in all publications are solely those of the individual author(s) and contributor(s) and not of MDPI and/or the editor(s). MDPI and/or the editor(s) disclaim responsibility for any injury to people or property resulting from any ideas, methods, instructions or products referred to in the content.